LETTER

doi:10.1038/nature13971

Isotopic constraints on marine and terrestrial N_2O emissions during the last deglaciation

Adrian Schilt[1,2], Edward J. Brook[1], Thomas K. Bauska[1], Daniel Baggenstos[3], Hubertus Fischer[2], Fortunat Joos[2], Vasilii V. Petrenko[4], Hinrich Schaefer[5], Jochen Schmitt[2], Jeffrey P. Severinghaus[3], Renato Spahni[2] & Thomas F. Stocker[2]

Nitrous oxide (N_2O) is an important greenhouse gas and ozone-depleting substance that has anthropogenic as well as natural marine and terrestrial sources[1]. The tropospheric N_2O concentrations have varied substantially in the past in concert with changing climate on glacial–interglacial and millennial timescales[2–8]. It is not well understood, however, how N_2O emissions from marine and terrestrial sources change in response to varying environmental conditions. The distinct isotopic compositions of marine and terrestrial N_2O sources can help disentangle the relative changes in marine and terrestrial N_2O emissions during past climate variations[4,9,10]. Here we present N_2O concentration and isotopic data for the last deglaciation, from 16,000 to 10,000 years before present, retrieved from air bubbles trapped in polar ice at Taylor Glacier, Antarctica. With the help of our data and a box model of the N_2O cycle, we find a 30 per cent increase in total N_2O emissions from the late glacial to the interglacial, with terrestrial and marine emissions contributing equally to the overall increase and generally evolving in parallel over the last deglaciation, even though there is no a priori connection between the drivers of the two sources. However, we find that terrestrial emissions dominated on centennial timescales, consistent with a state-of-the-art dynamic global vegetation and land surface process model that suggests that during the last deglaciation emission changes were strongly influenced by temperature and precipitation patterns over land surfaces. The results improve our understanding of the drivers of natural N_2O emissions and are consistent with the idea that natural N_2O emissions will probably increase in response to anthropogenic warming[11].

Ice-core studies indicate that during the past 800 kyr tropospheric N_2O concentrations ranged from about 200 to 300 p.p.b., covarying with climate on glacial–interglacial and millennial timescales (refs 2–8 and Fig. 1a). Pre-industrial atmospheric N_2O concentrations were regulated by microbiological production in marine and terrestrial environments and by photochemical destruction in the stratosphere[1]. Simulations suggest that the pre-industrial atmospheric lifetime of 142 ± 14 yr (ref. 12) remained relatively constant over the last deglaciation[13,14], and, therefore, past atmospheric N_2O concentrations were mainly modulated by emission strength. Importantly, emission strength increases in a warmer climate, implying that natural ecosystem N_2O production constitutes a positive climate feedback that will add to the anthropogenic N_2O load in the atmosphere and amplify the warming in coming centuries. However, the details of the relative sensitivities of marine and terrestrial sources to changing environmental conditions are not known at present, hampering quantitative projections of future emissions.

Modern field data indicate that marine and terrestrial N_2O emissions exhibit distinct isotopic compositions (Extended Data Fig. 1), with marine N_2O being more enriched in both heavy isotopes ($\delta^{15}N$ of 4–12‰ relative to atmospheric N_2; $\delta^{18}O$ of 42–67‰ relative to VSMOW) than is terrestrial N_2O ($\delta^{15}N$ of −34–2‰; $\delta^{18}O$ of 20–43‰). Therefore, the isotopic composition of tropospheric N_2O is a powerful tool for disentangling the relative changes of marine and terrestrial N_2O emissions during past climate variations[4,9,10]. For instance, decreasing tropospheric $\delta^{15}N$ and $\delta^{18}O$ indicate increasing importance of terrestrial emissions, whereas increasing $\delta^{15}N$ and $\delta^{18}O$ indicate increasing importance of marine emissions. The only prior study of the N_2O isotopic composition over the last deglaciation[4] found minimal change in the ratio of marine to terrestrial N_2O emissions, but was hindered by the relatively low temporal sampling resolution and precision of the measurements.

We determined the concentration and the isotopic composition of N_2O over the last deglaciation from 16–10 kyr before present (BP, AD 1950) (Fig. 1b) from a total of 64 ice samples collected along a horizontal transect on the Taylor Glacier, Antarctica (D.B. *et al.*, manuscript in preparation). Measurement precision, as determined by replicate analyses and reported here as pooled standard deviations (1σ), was 3.4 p.p.b. for the N_2O concentration, 0.28‰ for $\delta^{15}N$ and 1.04‰ for $\delta^{18}O$. The mean temporal sampling resolution was better than 100 yr. The timescale was established by synchronizing the fast global changes in tropospheric methane (CH_4) concentrations in the Taylor Glacier data with the corresponding data of the WAIS Divide deep ice core on an updated version of the WDC06A-7 timescale[15], with further constraints from the isotopic composition of atmospheric molecular oxygen between fast CH_4 changes (Methods). Note that atmospheric data extracted from polar ice samples are a smoothed representation of the atmospheric history owing to the mixing of air in the firn column; Taylor Glacier is expected to have a gas age distribution with a range of about 300 yr, similar to the Taylor Dome ice core[16]. The new Taylor Glacier N_2O isotopic data ($\delta^{15}N$ and $\delta^{18}O$) measured at Oregon State University agree with the only previously published N_2O isotopic data covering the last deglaciation, from the Taylor Dome ice core[4], as well as with new measurements performed at the University of Bern on ice samples from the Taylor Glacier and the Talos Dome ice core (Extended Data Fig. 2 and Methods). Taylor Glacier measurements confirm the trends in tropospheric N_2O concentrations from previous ice-core studies[2–5], and show the following general features in high temporal sampling resolution (Fig. 1b): N_2O rapidly increased from 211 ± 1 p.p.b. (mean ± s.e. in the time interval 15.9–14.9 kyr BP) during Heinrich stadial 1 (HS1) to 263 ± 2 p.p.b. (14.3–13.0 kyr BP) during the Bølling–Allerød interstadial. Following a decrease to 243 ± 2 p.p.b. (12.6–11.7 kyr BP) during the Younger Dryas stadial, N_2O reached 267 ± 1 p.p.b. (11.3–9.9 kyr BP) during the Preboreal stage. $\delta^{15}N$ averaged 10.3 ± 0.1‰ over the last deglaciation, with excursions of up to about 2‰. Approximately similar values were reached during HS1, the Younger Dryas and the Preboreal (10.3 ± 0.1‰), but $\delta^{15}N$ was higher during the Bølling–Allerød (10.7 ± 0.1‰). $\delta^{18}O$ averaged 45.5 ± 0.1‰ over the last deglaciation, with the magnitude of variability roughly similar to the precision of the measurements.

The robust isotopic variations in the new Taylor Glacier data reveal how the major environmental changes during the last deglaciation perturbed the nitrogen cycle and N_2O production. Broadly, the N_2O concentration data imply an increase in total N_2O emissions of about 30% from the late glacial to the interglacial, and the similar isotopic values

[1]College of Earth, Ocean, and Atmospheric Sciences, Oregon State University, Corvallis, Oregon 97331, USA. [2]Climate and Environmental Physics, Physics Institute, and Oeschger Centre for Climate Change Research, University of Bern, 3012 Bern, Switzerland. [3]Scripps Institution of Oceanography, University of California, San Diego, California 92037, USA. [4]Department of Earth and Environmental Sciences, University of Rochester, Rochester, New York 14627, USA. [5]National Institute of Water and Atmospheric Research, Wellington 6021, New Zealand.

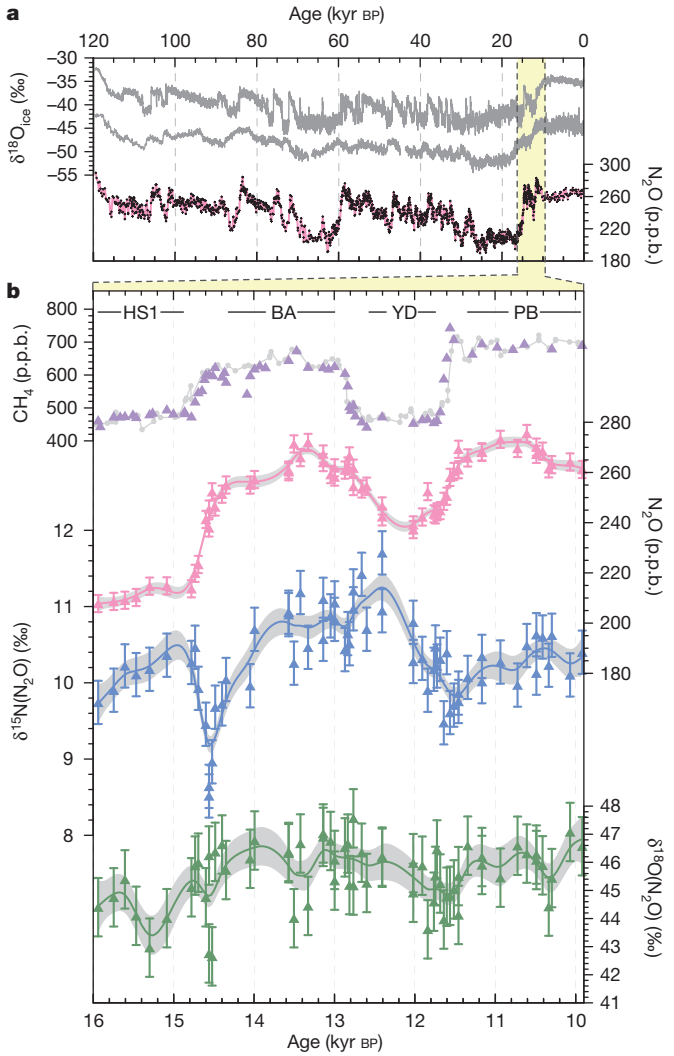

Figure 1 | Changes in tropospheric N_2O and climate proxies during the last glacial–interglacial cycle and the last deglaciation. **a,** The past 120 kyr on the AICC2012 timescale[26]: temperature proxies $\delta^{18}O_{ice}$ ($\delta^{18}O_{ice} = ((^{18}O/^{16}O)_{sample}/(^{18}O/^{16}O)_{VSMOW} - 1) \times 1{,}000‰$; VSMOW, Vienna Standard Mean Ocean Water) of Greenland (upper grey curve; North Greenland Ice Core Project[27]) and Antarctica (lower grey curve; EPICA Dronning Maud Land[28]), as well as tropospheric N_2O (pink; EPICA Dome C[29] and North Greenland Ice Core Project[3,5,8]). **b,** Detailed data from the last deglaciation from 16 to 10 kyr BP on an updated version of the WDC06A-7 timescale[15] (Methods): Taylor Glacier CH_4 (purple triangles) together with Talos Dome CH_4 (grey circles[30]), Taylor Glacier N_2O (pink), as well as $\delta^{15}N$ ($\delta^{15}N = ((^{15}N/^{14}N)_{sample}/(^{15}N/^{14}N)_{atmospheric\ N_2} - 1) \times 1{,}000‰$) (blue) and $\delta^{18}O$ (green; relative to VSMOW) of N_2O. Solid lines show splines with a cut-off period of 600 yr through the N_2O concentration and isotopic composition data. Error bars indicate pooled standard deviations of replicates ($\pm 1\sigma$, $n = 10$); grey shaded areas indicate $\pm 1\sigma$ envelopes from the Monte Carlo approach (Methods). BA, Bølling–Allerød; YD, Younger Dryas; PB, Preboreal.

during HS1 and the Preboreal indicate that both marine and terrestrial emissions contributed about equally to the overall increase. However, variations in the isotopic composition related to climate oscillations on millennial and centennial timescales during the last deglaciation point to substantially asynchronous responses of marine and terrestrial emissions on shorter timescales. The variations can be attributed to various drivers, such as changes in oxygen inventories and circulation in the global oceans, as well as changes in temperature and precipitation patterns over land. For instance, higher $\delta^{15}N$ during most of the Bølling–Allerød indicates relatively strong marine emissions, whereas the short-term decrease in $\delta^{15}N$ at the beginning of the Bølling–Allerød points to a fast increase in terrestrial emissions that preceded the increase in marine emissions.

To estimate the evolution of total N_2O emissions as well as the relative contributions of marine and terrestrial ecosystems over the last deglaciation on the basis of the Taylor Glacier data, we used a two-box model of atmospheric N_2O and its isotopic composition (Fig. 2). The model included a well-mixed troposphere and stratosphere, separate marine and terrestrial N_2O sources, and a stratospheric sink (Methods). Investigations with a more complex formulation of the box model including an explicit representation of the marine N_2O cycle and inventory suggest that the physical effects of air–sea interactions and ocean mixing on N_2O can be neglected on the timescales of the last deglaciation (Extended Data Fig. 3). We derived plausible emission histories using only the N_2O concentration and $\delta^{15}N$ data (which offered a higher signal-to-noise ratio than the $\delta^{18}O$ data); however, the results were consistent *post hoc* with the $\delta^{18}O$ constraints (Extended Data Fig. 4). The large range of the isotopic values for both marine and terrestrial N_2O emissions observed in modern field data (Extended Data Fig. 1) precluded a quantification of the exact marine and terrestrial fractions of the total emissions based on the measured tropospheric isotopic values. Notably, the reported late pre-industrial (AD 1750) $\delta^{15}N$ value[17] is similar to the Taylor Glacier value at 16 kyr BP (Fig. 2), suggesting similar relative strengths of marine and terrestrial N_2O emissions for pre-industrial and late glacial climate conditions. We therefore prescribed an initial marine fraction of 37% (that is, an initial terrestrial fraction of 63%) of the total emissions at 16 kyr BP, in line with best estimates for the modern natural N_2O budget[1]. The sensitivity of our results to the chosen relative strength of marine and terrestrial emissions at 16 kyr BP is illustrated by further scenarios with low and high estimates of the initial marine fraction of 17% and 74% (ref. 1), demonstrating that for all scenarios the marine and terrestrial fractions showed similar trends with absolute changes of only 7% or less over the last deglaciation (Extended Data Fig. 5). The box model accounts for atmospheric imbalances (non-steady-state conditions) affecting the tropospheric concentrations and isotopic compositions at times of rapidly changing atmospheric N_2O load (Methods). However, only a small part of the observed changes in N_2O and $\delta^{15}N$ were caused by such atmospheric imbalances, indicating that changes in marine and terrestrial emissions were mostly responsible for the observed variability in the Taylor Glacier data (Fig. 2). Our approach assumes that the isotopic compositions of marine and terrestrial N_2O emissions remained constant over time. For the marine source, support for this assumption comes from the observation that the global mean isotopic composition of bioavailable nitrogen did not change significantly over the last deglaciation[18]. For the terrestrial source, a global compilation of lacustrine $\delta^{15}N$ sedimentary data[19] does not reveal substantial changes, for example in response to the Younger Dryas. However, a long-term decrease with a rate of 0.25‰ per millennium is observed from 15 to 7 kyr BP; if transferred directly to the isotopic composition of the terrestrial N_2O source, this decrease would require an increase in marine emissions at the expense of terrestrial emissions of about 0.05 Tg N yr^{-1} per millennium to keep the isotopic composition of the troposphere constant. Although not negligible, this would still be small compared with the inferred changes in total N_2O emissions, which are of the order of 2.3 Tg N yr^{-1}.

Today, the strongest marine N_2O emissions occur in the eastern tropical and northern Pacific Ocean, the Southern Ocean, the Arabian Sea, and in coastal and equatorial upwelling regions, as inferred from inverse modelling[20]. High N_2O production rates in these regions and in the global ocean as a whole are closely linked to hypoxia (low concentrations of dissolved oxygen), which is controlled by the temperature- and salinity-dependent oxygen solubility, the cycling of organic matter, the availability of nutrients and, thus, ocean circulation. Indeed, ocean models suggest that a weakening of the Atlantic meridional overturning circulation (AMOC) leads to a decrease in marine N_2O production almost everywhere in the global oceans, in particular in the low-oxygen regions, because of higher stratification, increased oceanic storage of

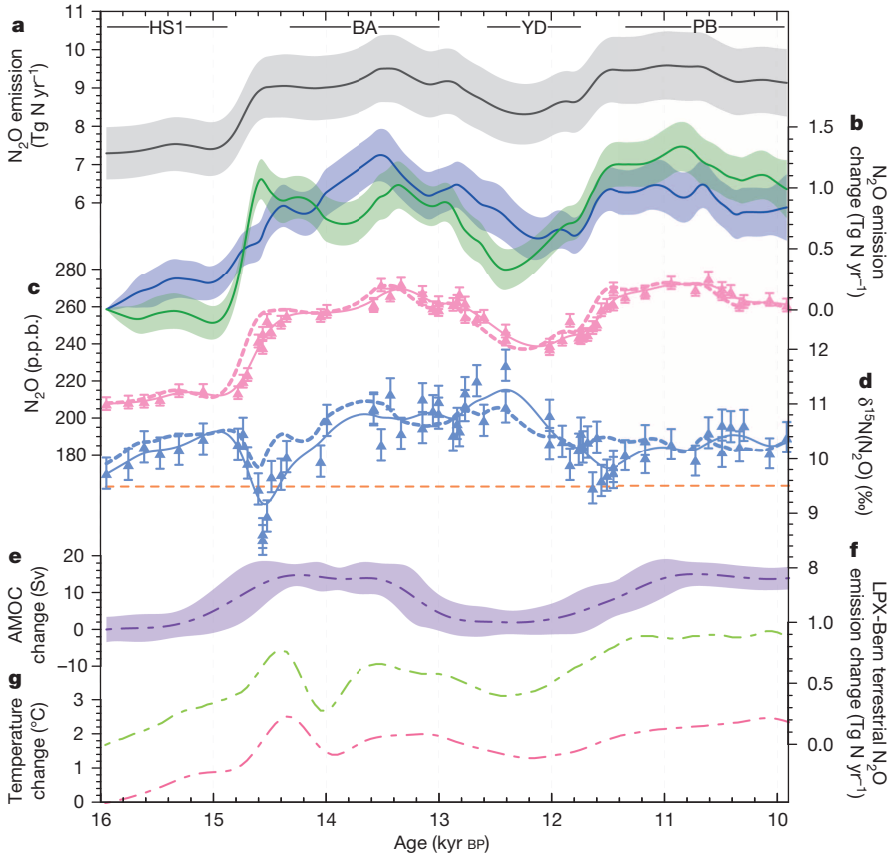

Figure 2 | N_2O emissions during the last deglaciation. **a,** Total N_2O emissions. **b**, Marine (blue) and terrestrial (green) N_2O emission changes relative to 16 kyr BP. Total, marine and terrestrial emissions were inversely calculated using the box model such that they recover the Taylor Glacier N_2O and $\delta^{15}N$ splines (solid lines in **c** and **d**, respectively) in a forward calculation. The uncertainty bands related to the emissions result from the Monte Carlo approach and indicate $\pm 1\sigma$ of all solutions. The absolute changes in marine and terrestrial emissions depend on the initial marine fraction, which was set to 37% of the total emissions at 16 kyr BP (see Extended Data Fig. 5 for sensitivity studies). **c**, Taylor Glacier N_2O, with $\pm 1\sigma$ error bars. **d**, Taylor Glacier $\delta^{15}N$ of N_2O, with $\pm 1\sigma$ error bars. The orange dashed line indicates pre-industrial (AD 1750) $\delta^{15}N$ (ref. 17). The dashed pink (**c**) and blue (**d**) lines show N_2O and $\delta^{15}N$ calculated using the modelled marine and terrestrial emissions but assuming equilibrium with respect to the sink at any time (Methods); the differences between solid and dashed lines indicate the effect of atmospheric imbalances. **e**, AMOC changes estimated using the Bern3D Earth System Model (including the $\pm 1\sigma$ uncertainty band), constrained by proxy data[23]. **f**, Terrestrial N_2O emission changes independently inferred from LPX-Bern. **g**, TraCE-21ka temperature changes over land surfaces[25] used to force LPX-Bern.

N_2O, less upwelling of nutrients into the euphotic zone, decreased primary productivity and increased subsurface oxygen concentrations impeding N_2O production[21,22].

The changes in marine N_2O emissions inferred from the Taylor Glacier data thus reflect important aspects of the globally integrated physical and biogeochemical ocean response to changing climate conditions. Reconstructions of AMOC changes[23] and the qualitative evolution of the marine oxygen inventory from a compilation of globally distributed marine sediment cores[24] can be combined with our data to provide a consistent history of marine N_2O emissions coupled to oxygen concentrations in the upper ocean. During the transition from HS1 to the Bølling–Allerød, the marine sediment data indicate a large expansion of hypoxia almost everywhere in the upper ocean, including the northern parts of the Pacific and Indian oceans, which are important regions for marine N_2O emissions[20]. Our reconstructions show that marine emissions substantially contributed to the concentration increase from 211 to 263 p.p.b. during that time (Fig. 2 and Extended Data Fig. 5); however, terrestrial emissions were similarly important (see below). During the Younger Dryas, the decrease in marine N_2O emissions occurred in concert with the weakening of the AMOC[23] as expected from model simulations[21,22]. N_2O concentrations reached slightly higher values during the Preboreal than during the Bølling–Allerød, whereas marine N_2O emissions were probably highest during the Bølling–Allerød, as also reflected by the oxygen availability in the global oceans reaching its lowest value during that time[24]. In contrast, terrestrial N_2O emissions were probably stronger during the Preboreal than during the Bølling–Allerød (Fig. 2), which may indicate that climate conditions on land increasingly favoured terrestrial N_2O emissions throughout the last deglaciation (interrupted by the Younger Dryas). This is indirectly supported by the observation that CH_4, which is controlled primarily by temperature- and precipitation-driven terrestrial sources, was also higher during the Preboreal than during the Bølling–Allerød (Fig. 1b). Although the general trends in marine and terrestrial N_2O emissions were coupled over the last deglaciation, confirming that both sources substantially contributed to the observed concentration increase[4], there are important differences on shorter timescales (Fig. 2). Notably, at the beginning of the Bølling–Allerød, the strong decrease in $\delta^{15}N$ suggests that terrestrial emissions increased more rapidly than did marine emissions, and reached an early maximum between 15 and 14 kyr BP.

For an independent comparison with the reconstructed emissions inferred from the Taylor Glacier data, we simulated terrestrial N_2O emissions using LPX-Bern, a dynamic global vegetation and land surface process model[11] (Methods). LPX-Bern was forced with climate anomalies from the TraCE-21ka experiment, a general circulation model simulation of climate over the last deglaciation with orbital, greenhouse gas, ice-sheet and meltwater forcings[25]. The LPX-Bern simulations qualitatively reproduce the reconstructed trends as well as variations on millennial and centennial timescales in terrestrial N_2O emissions

over the last deglaciation, including the early maximum between 15 and 14 kyr BP, the decrease from the Bølling–Allerød into the Younger Dryas, and the subsequent increase into the Preboreal to values slightly above those of the Bølling–Allerød (Fig. 2). The simulated emission changes in LPX-Bern are strongly influenced by temperature (and precipitation) patterns over land surfaces, suggesting that those parameters contributed to the variability in terrestrial N_2O emissions over the last deglaciation. The qualitative agreement between the reconstructed and modelled emissions, coupled with the apparent sensitivity of N_2O emissions to temperature in both the model simulation and ice-core data, strongly suggests that terrestrial emissions acted as a positive feedback on climate change during the last deglaciation.

Our results provide insight into the nitrogen cycle and the overall functioning of marine and terrestrial ecosystems under varying environmental conditions, and are consistent with the hypothesis that natural N_2O emissions will probably increase in response to anthropogenic warming. The results also increase confidence in the ability of present-generation dynamic global vegetation and land surface process models to project changes in terrestrial N_2O emissions in response to climate change.

Online Content Methods, along with any additional Extended Data display items and Source Data, are available in the online version of the paper; references unique to these sections appear only in the online paper.

Received 24 March; accepted 13 October 2014.

1. Stocker, T. F. *et al.* (eds) *Climate Change 2013: The Physical Science Basis* (Cambridge Univ. Press, 2013).
2. Flückiger, J. *et al.* Variations in atmospheric N_2O concentration during abrupt climatic changes. *Science* **285,** 227–230 (1999).
3. Schilt, A. *et al.* The response of atmospheric nitrous oxide to climate variations during the last glacial period. *Geophys. Res. Lett.* **40,** 1888–1893 (2013).
4. Sowers, T., Alley, R. B. & Jubenville, J. Ice core records of atmospheric N_2O covering the last 106,000 years. *Science* **301,** 945–948 (2003).
5. Schilt, A. *et al.* Atmospheric nitrous oxide during the last 140,000 years. *Earth Planet. Sci. Lett.* **300,** 33–43 (2010).
6. Spahni, R. *et al.* Atmospheric methane and nitrous oxide of the late Pleistocene from Antarctic ice cores. *Science* **310,** 1317–1321 (2005).
7. Schilt, A. *et al.* Glacial-interglacial and millennial-scale variations in the atmospheric nitrous oxide concentration during the last 800,000 years. *Quat. Sci. Rev.* **29,** 182–192 (2010).
8. Flückiger, J. *et al.* N_2O and CH_4 variations during the last glacial epoch: insight into global processes. *Glob. Biogeochem. Cycles* **18,** GB1020 (2004).
9. Ishijima, K. *et al.* Temporal variations of the atmospheric nitrous oxide concentration and its $\delta^{15}N$ and $\delta^{18}O$ for the latter half of the 20th century reconstructed from firn air analyses. *J. Geophys. Res.* **112,** D03305 (2007).
10. Röckmann, T., Kaiser, J. & Brenninkmeijer, C. A. M. The isotopic fingerprint of the pre-industrial and the anthropogenic N_2O source. *Atmos. Chem. Phys.* **3,** 315–323 (2003).
11. Stocker, B. D. *et al.* Multiple greenhouse-gas feedbacks from the land biosphere under future climate change scenarios. *Nature Clim. Change* **3,** 666–672 (2013).
12. Prather, M. J., Holmes, C. D. & Hsu, J. Reactive greenhouse gas scenarios: systematic exploration of uncertainties and the role of atmospheric chemistry. *Geophys. Res. Lett.* **39,** L09803 (2012).
13. Crutzen, P. J. & Bruhl, C. A model study of atmospheric temperatures and the concentrations of ozone, hydroxyl, and some other photochemically active gases during the glacial, the preindustrial Holocene and the present. *Geophys. Res. Lett.* **20,** 1047–1050 (1993).
14. Martinerie, P., Brasseur, G. P. & Granier, C. The chemical composition of ancient atmospheres: a model study constrained by ice core data. *J. Geophys. Res.* **100,** 14291–14304 (1995).
15. Wais Divide Project Members. Onset of deglacial warming in West Antarctica driven by local orbital forcing. *Nature* **500,** 440–444 (2013).
16. Indermühle, A. *et al.* Atmospheric CO_2 concentration from 60 to 20 kyr BP from the Taylor Dome Ice Core, Antarctica. *Geophys. Res. Lett.* **27,** 735–738 (2000).
17. Bernard, S. *et al.* Constraints on N_2O budget changes since pre-industrial time from new firn air and ice core isotope measurements. *Atmos. Chem. Phys.* **6,** 493–503 (2006).
18. Galbraith, E. D., Kienast, M. & The NICOPP working group members. The acceleration of oceanic denitrification during deglacial warming. *Nature Geosci.* **6,** 579–584 (2013).
19. McLauchlan, K. K., Williams, J. J., Craine, J. M. & Jeffers, E. S. Changes in global nitrogen cycling during the Holocene epoch. *Nature* **495,** 352–355 (2013).
20. Hirsch, A. I. *et al.* Inverse modeling estimates of the global nitrous oxide surface flux from 1998–2001. *Glob. Biogeochem. Cycles* **20,** GB1008 (2006).
21. Goldstein, B., Joos, F. & Stocker, T. F. A modeling study of oceanic nitrous oxide during the Younger Dryas cold period. *Geophys. Res. Lett.* **30,** 1092 (2003).
22. Schmittner, A. & Galbraith, E. D. Glacial greenhouse-gas fluctuations controlled by ocean circulation changes. *Nature* **456,** 373–376 (2008).
23. Ritz, S. P. *et al.* Estimated strength of the Atlantic overturning circulation during the last deglaciation. *Nature Geosci.* **6,** 208–212 (2013).
24. Jaccard, S. L. & Galbraith, E. D. Large climate-driven changes of oceanic oxygen concentrations during the last deglaciation. *Nature Geosci.* **5,** 151–156 (2012).
25. Liu, Z. *et al.* Transient simulation of last deglaciation with a new mechanism for Bølling-Allerød warming. *Science* **325,** 310–314 (2009).
26. Veres, D. *et al.* The Antarctic ice core chronology (AICC2012): an optimized multi-parameter and multi-site dating approach for the last 120 thousand years. *Clim. Past* **9,** 1733–1748 (2013).
27. NGRIP Members. High-resolution record of Northern Hemisphere climate extending into the last interglacial period. *Nature* **431,** 147–151 (2004).
28. EPICA Community Members. One-to-one coupling of glacial climate variability in Greenland and Antarctica. *Nature* **444,** 195–198 (2006).
29. Flückiger, J. *et al.* High-resolution Holocene N_2O ice core record and its relationship with CH_4 and CO_2. *Glob. Biogeochem. Cycles* **16,** 1010 (2002).
30. Stenni, B. *et al.* Expression of the bipolar see-saw in Antarctic climate records during the last deglaciation. *Nature Geosci.* **4,** 46–49 (2011).

Acknowledgements Financial support was provided by the Swiss National Science Foundation (NSF) and the US NSF, including a Swiss NSF Fellowship for Prospective Researchers (139404) to A.S., US NSF Grant PLR08-38936 to E.J.B. and US NSF Grant PLR08-39031 to J.P.S. Further support came from the Marsden Fund Council from New Zealand Government funding, administered by the Royal Society of New Zealand. We thank C. Buizert, X. Faïn, J. Lee, L. Mitchell and P. Rose for fieldwork, R. Roth for providing the Bern3D Earth System Model run, J. Schwander for providing the NEEM firn air cylinder, S. Jaccard for comments and A. Ross for lab assistance. We thank B. Otto-Bliesner and Z. Liu for providing climate data from the TraCE-21ka model computation, which was carried out at the Oak Ridge Leadership Computational Facility, sponsored by the US Department of Energy, and the National Center for Atmospheric Research Supercomputing Facility, sponsored by the US NSF. The TraCE-21ka project was supported by the US NSF and the US Department of Energy.

Author Contributions J.P.S., V.V.P. and E.J.B. initiated and led the Taylor Glacier project. T.K.B., E.J.B., D.B., V.V.P., H.S., A.S. and J.P.S. performed fieldwork. A.S. set up the experimental apparatus for N_2O isotopes and carried out the measurements, with great support from T.K.B., E.J.B. and J.S. Intercomparison measurements were performed by J.S. at the University of Bern and by T.K.B. at Oregon State University. D.B. and T.K.B. developed the timescale for Taylor Glacier. A.S. and F.J. performed the box modelling. R.S. and F.J. produced and interpreted the LPX-Bern model results. All authors discussed the results and contributed to the manuscript, which was written by A.S.

Author Information Reprints and permissions information is available at www.nature.com/reprints. The authors declare no competing financial interests. Readers are welcome to comment on the online version of the paper. Correspondence and requests for materials should be addressed to A.S. (adrian.schilt@gmail.com).

METHODS

Standard gases for N_2O concentration and isotopic composition. To date, no official international standard gases exist for the isotopic composition of N_2O, and isotopic results are instead reported directly on the internationally accepted atmospheric N_2 (for $\delta^{15}N$) and VSMOW (for $\delta^{18}O$) scales. For practical reasons it is advantageous to have a standard gas consisting of N_2O in air at tropospheric concentration. Therefore, a standard gas cylinder of tropospheric background air, labelled NOAA-1, filled on 11 December 2008 at Niwot Ridge, Colorado, was used as the primary standard at Oregon State University. The N_2O concentration was 322.32 ± 0.14 p.p.b. according to a calibration by the National Oceanic and Atmospheric Administration (NOAA-2006A scale). The isotopic composition was expressed in the customary delta notation, that is, $\delta^{15}N = ({}^{15}R_{sample}/{}^{15}R_{standard} - 1) \times 1{,}000‰$ and $\delta^{18}O = ({}^{18}R_{sample}/{}^{18}R_{standard} - 1) \times 1{,}000‰$ with R_{sample} and $R_{standard}$ respectively being the ratios of heavy to light isotopes of the sample and the corresponding standard (atmospheric N_2 for $\delta^{15}N$ and VSMOW for $\delta^{18}O$). To assign $\delta^{15}N$ and $\delta^{18}O$ values to NOAA-1, the recently published N_2O isotopic data spanning the years 1978–2005 retrieved from archived air samples from Cape Grim, Tasmania[31], were linearly extrapolated to the collection date of NOAA-1 (Extended Data Fig. 6). This assignment led to $\delta^{15}N$ and $\delta^{18}O$ values for NOAA-1 of 6.18‰ and 44.16‰, respectively. To test this empirical calibration, a second standard gas cylinder, labelled NOAA-2, filled on 5 October 1988 at Niwot Ridge was used. Its analysis relative to NOAA-1 resulted in respective $\delta^{15}N$ and $\delta^{18}O$ values of 6.93 ± 0.04‰ and 44.29 ± 0.07‰, and a N_2O concentration of 306.9 ± 0.3 p.p.b. (mean ± s.e., $n = 8$). The linear interpolation of the Cape Grim data would lead to respective $\delta^{15}N$ and $\delta^{18}O$ values of 6.91‰ and 44.62‰, and a N_2O concentration of 307.1 p.p.b., suggesting a reasonably good agreement within the interannual scatter of the Cape Grim data (Extended Data Fig. 6). As a further test of the calibration scale, and to allow for comparison with future data sets, firn air collected on 27 July 2008 at NEEM, Greenland (dated to approximately AD 1958), was analysed both at Oregon State University and the University of Bern. On average, the $\delta^{15}N$ and $\delta^{18}O$ values measured at Oregon State University were 0.80‰ lower and 0.36‰ higher, respectively, than the values measured at the University of Bern, where an independent primary standard, calibrated with a similar method[32], was used. These differences were again within the range of the interannual scatter observed in the Cape Grim data. Because the isotopic composition of NOAA-1 used as the standard differed from the values measured in the ice samples, a small systematic bias in the absolute values cannot entirely be ruled out, even though the Taylor Glacier data are in good agreement with data from other labs (Extended Data Fig. 2). However, a systematic bias in the reference scale would not affect the conclusions drawn in this manuscript. Finally, an artificial air mixture, labelled NOAA-3, with a N_2O concentration of 283.25 ± 0.09 p.p.b. was available at Oregon State University for additional calibrations and for quality assurance (see below).

Measurement procedure for N_2O concentration and isotopic composition. The analysis of the nitrogen and oxygen isotopic composition of N_2O ($\delta^{15}N$ and $\delta^{18}O$) was performed in a fashion similar to previously described techniques[32–35] using a MAT 253 isotope mass spectrometer in continuous-flow mode, which was coupled to a pre-concentration device and a gas chromatograph. The ancient air was extracted from Taylor Glacier ice samples containing visible air bubbles using two 'cheese grater' devices, that is, electropolished, stainless-steel extraction pots (4.7 l) equipped with perforated, electropolished, stainless-steel plates with sharp edges[36]. Before the ice samples were loaded, the extraction pots were washed with Milli-Q water and ethanol, completely dried at 60 °C (45–60 min) and cooled in a walk-in freezer (about 60 min) to the temperature of the stored ice samples (−25 °C). Taylor Glacier ice samples were cut and cleaned (by removing typically about 200 g of the outermost ice) with a bandsaw, resulting in octagonal prisms of about 700–900 g. The loaded extraction pots were sealed with copper gaskets (CF flange), put inside the lab freezer at −60 °C and evacuated for 30 min. The next day, the first extraction pot was evacuated for another 45 min and then the first ice sample was grated by moving the extraction pot back and forth horizontally for one hour in the lab freezer at −60 °C. On average 36% of the ice sample was grated and about 20–40 ml of air was typically extracted. The rather low grating efficiency did not affect the results, because intact ice remained and bubbles were either completely opened or remained closed (the results were also confirmed by intercalibration measurements using a different extraction technique; see below). The air was then expanded into the vacuum system, where traps were installed in the following sequential order: (i) a stainless-steel, 1/4-inch tube forming a spiral at −105 °C, to trap water vapour; (ii) a stainless-steel, 1/4-inch tube forming a double U-trap at liquid-nitrogen temperature, to trap N_2O and CO_2; and (iii) a 1/4-inch cold finger at 11 K, acting as a vacuum pump and trapping the remaining air constituents in about 21 min. By transferring N_2O and CO_2 with a helium flow (47 ml min^{-1}; ultrapure helium additionally cleaned with a hydrocarbon trap, a high-capacity gas purifier and an indicating hydrocarbon, moisture and oxygen trap) through an Ascarite and magnesium perchlorate trap, CO_2 was chemically removed and N_2O was further pre-concentrated in a stainless-steel, 1/16-inch tube forming a U-trap at liquid-nitrogen temperature. N_2O was then transferred with a helium flow (0.9 ml min^{-1}) onto a deactivated, fused-silica capillary (internal diameter, 0.25 mm) immersed in liquid nitrogen that served as a cryofocus. N_2O was separated from remaining traces of CO_2 in a fused-silica gas chromatographic column (Agilent PoraBond Q; internal diameter, 0.32 mm; 25 m) at 24 °C again using a helium flow (0.9 ml min^{-1}). After passing a Nafion dryer, N_2O entered the open split of a Thermo Scientific ConFlo IV and from there the MAT 253 isotope mass spectrometer, where the m/z 44, 45 and 46 beams were monitored. Direct injection of ultrapure N_2O into the open split produced four rectangular peaks of 20 s duration preceding the Gaussian peak eluting from the gas chromatographic column, the latter typically reaching peak areas of 0.7–1.6 V s for m/z 44. Before and after the ice-sample measurement, duplicates of similar chromatograms were produced by repeated pre-concentration of N_2O from an aliquot of NOAA-1 standard gas, resulting in peak areas of 2.5 V s for m/z 44. Furthermore, an additional NOAA-1 standard gas measurement not used for calibration was performed at the beginning to test and condition the measurement system. After baseline correction and peak integration of both the rectangular and Gaussian peaks in each chromatogram using a custom-designed algorithm able to fit exponential baselines, the elemental ratios of each peak were calculated, thereby correcting for the contribution of ^{17}O according to ref. 37. Then the raw $\delta^{15}N$ and $\delta^{18}O$ values of the Gaussian peaks of each chromatogram were determined relative to the mean of the four preceding rectangular peaks. This ensured the removal of any potential drift of the mass spectrometer over the course of the measurement day. Finally, the raw $\delta^{15}N$ and $\delta^{18}O$ values of the ice-sample peak were referenced against the mean raw $\delta^{15}N$ and $\delta^{18}O$ values of the four NOAA-1 standard gas peaks. To determine the N_2O concentration, the air from the ice-sample and NOAA-1 standard gas measurements collected on separate cold fingers was expanded into a previously evacuated stainless-steel cylinder (2.4 l) installed inside the oven of the temperature-stable gas chromatograph, and the pressure was recorded. The N_2O concentration of the ice sample was then calculated by referencing the m/z 44 peak area-to-pressure ratio of the ice-sample measurement against the mean of the m/z 44 peak area-to-pressure ratios of the NOAA-1 standard gas measurements. Finally, the evacuation, grating and measuring procedures were repeated with the second extraction pot to measure two ice samples per day.

Long-term stability, amount dependency and blank ice measurements. To ensure that the data resulting from a measurement series extending over several months were not affected by any systematic drift (for example that caused by unintended changes in the standard gases, pre-concentration system or measurement procedure), NOAA-3 standard gas was analysed daily with peak areas of 1.92 ± 0.05 V s for m/z 44. The results over the full measurement series showed no drift and the standard deviations (1σ, $n = 31$) were 0.14‰ and 0.32‰ for $\delta^{15}N$ and $\delta^{18}O$, respectively (Extended Data Fig. 7a). To investigate the amount dependency of the measurement system over the full range of analysed N_2O amounts (8.5–21.0 ng of N_2O), an aliquot of NOAA-1 standard gas containing the same amount of N_2O as the preceding ice sample was routinely analysed. The N_2O isotopic compositions of these measurements did not show a significant amount dependency (Extended Data Fig. 7b). Their standard deviations (1σ, $n = 58$) were 0.22‰ and 0.59‰ for $\delta^{15}N$ and $\delta^{18}O$, respectively, and were thus somewhat higher than the standard deviations of the NOAA-3 standard gas measurements used to check the stability of the system as mentioned above, probably owing to the smaller peak areas. Ten measurements of different amounts of NOAA-1 standard gas which was stored in the extraction pots while a piece of artificial bubble-free ice was grated further confirmed the absence of a significant amount dependency of $\delta^{15}N$ and $\delta^{18}O$ over the relevant range (Extended Data Fig. 7c). The mean and standard deviation for $\delta^{15}N$ were respectively 6.11‰ and 0.13‰, and, thus, similar to the value of 6.18‰ assigned to NOAA-1. However, the mean and standard deviation of $\delta^{18}O$ were respectively 42.78‰ and 0.70‰, and, thus, 1.38‰ lower than the value assigned to NOAA-1. Although the reasons for this offset remained obscure, the $\delta^{18}O$ data presented in this study were corrected by +1.38‰. The mean N_2O concentration was 323.2 ± 2.8 p.p.b., compared with 322.32 p.p.b. for the NOAA-1 standard gas. According to these results, N_2O concentration data were not corrected for any shift or amount dependency.

Sampling. In the austral summer 2011–2012, ice samples covering the last deglaciation were collected on the Taylor Glacier, Dry Valleys, Antarctica (77° 46′ S, 161° 43′ E), on a horizontal transect perpendicular to the flow line of the glacier ('horizontal ice core'; D.B. *et al.*, manuscript in preparation). To avoid cracks in the ice caused by thermal stress on the glacier surface, the ice samples were retrieved from a depth of about 4 m. The horizontal distance between ice samples was usually 1 m, and the transect covered a total distance of 276 m including a fold resulting from disturbed ice flow. The timescale was established by synchronization of fast global changes in the Taylor Glacier CH_4 data with the corresponding changes in the WAIS Divide deep ice-core CH_4 data on an updated version of the WDC06A-7 timescale[15]. Between these tie points the synchronization was further constrained by finding the optimal alignment of the Taylor Glacier and WAIS Divide deep ice-core isotopic data of molecular oxygen using a previously described matching technique[38]. On the resulting timescale, which will be presented in detail in forthcoming publications, the timing of major changes in CH_4, CO_2, N_2O and the isotopic composition of

molecular oxygen were in excellent agreement with previous ice-core data from Greenland and Antarctica. For instance, the Taylor Glacier CH_4 data matched the Talos Dome CH_4 data on the independent AICC2012 timescale[26] (Fig. 1). This study focuses on the time interval from 16 to 10 kyr BP because the quality and quantity of collected Taylor Glacier ice samples with greater ages did not allow for reliable N_2O measurements.

Analysis of Taylor Glacier ice samples. Sixty-four Taylor Glacier ice samples were analysed in random order for their N_2O concentrations and $\delta^{15}N$ and $\delta^{18}O$ isotopic compositions. These measurements included ten pairs of replicates, which had pooled standard deviations (1σ) of 3.4 p.p.b. for the N_2O concentration, 0.28‰ for $\delta^{15}N$ and 1.04‰ for $\delta^{18}O$. These standard deviations were considered to represent the best estimates of the measurement uncertainties, because the replicates were affected by most potential sources of disturbance (for example small-scale anomalies in the ice samples, drifts throughout the measurements series, uncertainties associated with baseline correction and peak integration, and so on). The final results were corrected for gravitational enrichment in the firn column on the basis of measurements of the isotopic composition of atmospheric molecular nitrogen using ice samples collected at the same site (D.B. *et al.*, manuscript in preparation). The corrections for all Taylor Glacier ice samples were relatively small and accounted for a reduction of 0.4-1.0 p.p.b. for N_2O, 0.12-0.24‰ for $\delta^{15}N$ and 0.24-0.50‰ for $\delta^{18}O$. Diffusive isotopic fractionation of N_2O in the firn at this site is negligible for the observed concentration increase rates[39].

Effect of atmospheric imbalances on the isotopic composition of tropospheric N_2O. Rapid changes in the atmospheric N_2O load lead to temporal shifts (lasting several lifetimes) in the isotopic composition of tropospheric N_2O even when the overall isotopic composition of the total N_2O source remains unchanged[40]. This is a consequence of the preferred removal of N_2O enriched in light isotopes by the stratospheric sink, which can also be described by a slightly longer atmospheric lifetime of N_2O enriched in heavy isotopes. Accordingly, a hypothetical rapid increase or decrease of global emissions without changing the overall isotopic composition of the emitted N_2O would still temporarily shift tropospheric $\delta^{15}N$ and $\delta^{18}O$ to lighter or, respectively, heavier values. Indeed, the Taylor Glacier data reveal that contemporaneously with the fast increases of the N_2O load from HS1 to the Bølling–Allerød as well as from the Younger Dryas to the Preboreal, $\delta^{15}N$ decreased rapidly, whereas it rapidly increased contemporaneously with the decrease of N_2O from the Bølling–Allerød to the Younger Dryas (Fig. 1b). The box model allowed for quantification of the atmospheric imbalances and shows that they explain only part of these observed trends, suggesting that the relative contributions of marine and terrestrial sources changed as well (Fig. 2). This is highlighted by calculation of the hypothetical N_2O concentration and $\delta^{15}N$ isotopic composition which would result when, at any time, the marine and terrestrial emissions reached equilibrium with the sink. The evolution of this equilibrated atmosphere is illustrated with dashed lines in Fig. 2; the differences between dashed and solid lines indicate the effect of atmospheric imbalances accounted for by the box model.

Atmospheric origin of Taylor Glacier N_2O data. Past studies of N_2O on air extracted from polar ice cores were often complicated by *in situ* production of N_2O in the ice matrix, which, for some ice cores, partly contaminated the atmospheric signal[2,3,5,8,33]. Although it is hard to rule out unambiguously any influence of *in situ* production on the new Taylor Glacier concentration and $\delta^{15}N$ and $\delta^{18}O$ data between 16 and 10 kyr BP, the following considerations point to an exclusively atmospheric origin of the reconstructed trends. First, although *in situ* production has been described as occurring randomly with large scatter between nearby ice samples[2,3,5,8,33], the Taylor Glacier N_2O concentration data are smooth and in complete agreement with independent measurements on a second set of ice samples from the same site produced with the apparatus for CO_2 isotopes at Oregon State University[36] (Extended Data Fig. 2), as well as with the atmospheric trends previously reconstructed along various ice cores. However, the fact that the Taylor Glacier ice samples were more than tenfold larger than the samples used for most concentration measurements may have obscured the detection of excess N_2O potentially present owing to *in situ* production on small spatial scales within Taylor Glacier ice samples. Second, the Taylor Glacier $\delta^{15}N$ and $\delta^{18}O$ data between 16 and 10 kyr BP do not show obvious outliers, and replicated measurements showed a satisfactory reproducibility; the standard deviations increased only from 0.22‰ to 0.28‰ for $\delta^{15}N$ and from 0.59‰ to 1.04‰ for $\delta^{18}O$ when measuring natural ice samples instead of standard gas, the latter being unaffected by the extraction process and potential variations in the ice. Third, $\delta^{15}N$ and $\delta^{18}O$ show short-term isotopic excursions partly resulting from imbalances in the emission and removal of N_2O at times of changing atmospheric N_2O load. Because these variations are an expected and well-understood consequence of atmospheric processes related to the preferred removal of N_2O enriched in light isotopes by the stratospheric sink, their presence in $\delta^{15}N$ provides confidence that the Taylor Glacier data indeed represent atmospheric trends.

Calculation of marine and terrestrial emissions (two-box model). To calculate the relative contributions of marine and terrestrial sources to total N_2O emissions, a two-box model (similar to refs 9, 10, 41), including a tropospheric and a stratospheric box, a marine and a terrestrial source, as well as a stratospheric sink, was used, with the basic equations shown in Extended Data Table 1. In a Monte Carlo approach, the model parameters (atmospheric lifetime, exchange rate of air between troposphere and stratosphere, stratospheric fractionation constant, and characteristic isotopic compositions of the marine and terrestrial sources) were randomly varied within prescribed distributions, which were based either on measurement uncertainties or the full ranges reported in the literature (Extended Data Table 2). For each random combination of parameters, the marine and terrestrial emissions that reproduce the Taylor Glacier N_2O concentration and $\delta^{15}N$ isotopic data (represented by splines with an empirical cut-off period of 600 yr, which smoothly follow the significant variability in the data) were inversely calculated. Hence, in a forward calculation the determined marine and terrestrial emissions would exactly recover the (splined) Taylor Glacier data. To take into account the measurement uncertainties, for each iteration the Taylor Glacier data were randomly varied within their uncertainties (Gaussian distributions using the pooled standard deviations of ten pairs of replicates), and the splines were re-determined. We argue that on the basis of the available data it is currently not possible to estimate robust global mean values for the isotopic compositions of the marine and terrestrial N_2O sources. Therefore, a conservative approach was used with distributions uniformly covering the full ranges of field data (Extended Data Fig. 1). The Monte Carlo simulations were continued until 500 combinations were found with initial marine fractions (at 16 kyr BP) of 17%, 37% and 74% of total emissions in respective accordance with low, best and high estimates for the modern natural N_2O budget[1] (Extended Data Fig. 5), ignoring all other results (with different initial marine fractions). Using the resulting evolutions of marine and terrestrial emissions to calculate tropospheric $\delta^{18}O$ provided results which were consistent with Taylor Glacier $\delta^{18}O$ for the scenarios with initial marine fractions of 17% and 37% (Extended Data Fig. 4). However, the scenario with an initial marine fraction of 74% was not supported by the isotopic data because it would require $\delta^{18}O$ values of the marine and terrestrial sources outside the range of reported field data (Extended Data Table 2). Finally, to estimate the effect of the marine N_2O cycle and inventory on tropospheric N_2O and $\delta^{15}N$, the two-box model was extended by six stacked ocean boxes. The timescales of exchange between the ocean boxes as well as between the uppermost ocean box and the troposphere were tuned to get the same model response to an instant emission of 200 Tg N into the troposphere as with the Bern3D Earth System Model[42]. Both formulations of the box model produced very similar results, indicating that, owing to the fast exchange of N_2O between the ocean and the atmosphere, any physical effects caused by ocean circulation and N_2O solubility can be neglected for the last deglaciation (Extended Data Fig. 3).

LPX-Bern model. For comparison with the terrestrial N_2O emissions inferred from the box model based on the Taylor Glacier data, terrestrial N_2O emissions over the last deglaciation were independently derived from transient simulations with LPX-Bern, a dynamic global vegetation and land surface process model. We applied the most recently published version of the model[11] (v1.0), with input data and set-up as published in ref. 43. The LPX-Bern model describes dynamical vegetation and terrestrial biogeochemical processes, and integrates representations of non-peatland[44–46] and peatland[43,47,48] ecosystems and their carbon and nitrogen dynamics[11,49,50]. The model calculates the release and uptake of the trace gases CO_2, N_2O (refs 11, 49, 50) and CH_4 (refs 51–53). Plant functional types (PFTs) are the basic biological units and represent different life forms (grasses, trees, mosses) and combinations of plant traits (needle-leaved, broad-leaved and so on). These PFTs are in competition for resources (water, light, nitrogen) on each grid cell and land unit (for example peat and non-peat). The model accounts for the coupling of carbon and water cycles through photosynthesis and evapotranspiration. It uses a vertically resolved soil hydrology, heat diffusion and an interactive thawing–freezing scheme[46,47]. The LPX-Bern vegetation component interacts with a dynamic nitrogen-cycle module that includes the relevant nitrogen fluxes and pools for plants and soils. The nitrogen source is implied by keeping the ratio of soil carbon to nitrogen constant over time. Thus, in LPX-Bern plant growth is not directly limited by external nitrogen input into an ecosystem, but by the rate of nitrogen remineralisation for a given climate. The total global N_2O emissions in LPX-Bern depend on the model parameters for the nitrogen fraction emitted as N_2O during denitrification and the fraction of nitrogen leaching in the form of N_2O in runoff. Although changes in soil texture over time could have an impact on terrestrial N_2O emissions[54], no information on soil texture changes over the last deglaciation is available and the modern field was applied, representing a potential source of uncertainty. The input climate (temperature, precipitation, cloud cover, wet days) was obtained from anomalies of transient climate simulations over the past 21 kyr with the NCAR CCSM3 (TraCE-21ka[25,55]) and observed present day climate (CRU[56]). Further input data were atmospheric CO_2 (ref. 57), orbital insolation changes[58] and topography changes through ice-sheet and sea-level changes imposed by ICE-5G[59]. Here the LPX-Bern model was run with a spatial resolution of $3.75^\circ \times 2.5^\circ$ and a daily time step was applied in the photosynthesis, water and nitrogen modules. Simulations started from an equilibrated spin-up at 21 kyr BP. Note that as we were

applying LPX-Bern as used in the literature, the absolute emissions at 16 kyr BP were 6.2 Tg N yr^{-1}, whereas the value corresponding to an initial marine fraction of 37% of the total source is 4.6 Tg N yr^{-1}. Several potential biases might explain differences in the magnitude of terrestrial N_2O emissions and emission changes inferred from LPX-Bern and the Taylor Glacier data: the initial terrestrial fraction (at 16 kyr BP) in the box model could be overestimated (Methods and Extended Data Fig. 5), the sensitivity of LPX-Bern to temperature changes could be too low (LPX-Bern shows a positive sensitivity to changes in temperature), or the temperature anomalies from TraCE-21ka could be damped relative to climate during the last deglaciation (TraCE-21ka indeed shows a relatively modest warming over the last deglaciation and modest changes associated with the Younger Dryas). However, the LPX-Bern simulations show reasonable quantitative emissions without any further tuning, and are used here as an independent approach to further support the variability in terrestrial N_2O emissions as inferred from the Taylor Glacier data.

31. Park, S. *et al.* Trends and seasonal cycles in the isotopic composition of nitrous oxide since 1940. *Nature Geosci.* **5,** 261–265 (2012).
32. Schmitt, J., Seth, B., Bock, M. & Fischer, H. Online technique for isotope and mixing ratios of CH_4, N_2O, Xe and mixing ratios of organic trace gases on a single ice core sample. *Atmos. Meas. Tech.* **7,** 2645–2665 (2014).
33. Sowers, T. N_2O record spanning the penultimate deglaciation from the Vostok ice core. *J. Geophys. Res.* **106,** 31903–31914 (2001).
34. Sapart, C. J. *et al.* Simultaneous stable isotope analysis of methane and nitrous oxide on ice core samples. *Atmos. Meas. Tech.* **4,** 2607–2618 (2011).
35. Sperlich, P. *et al.* An automated GC-C-GC-IRMS setup to measure palaeoatmospheric $\delta^{13}C$-CH_4, $\delta^{15}N$-N_2O and $\delta^{18}O$-N_2O in one ice core sample. *Atmos. Meas. Tech.* **6,** 2027–2041 (2013).
36. Bauska, T. K., Brook, E. J., Mix, A. C. & Ross, A. High-precision dual-inlet IRMS measurements of the stable isotopes of CO_2 and the N_2O/CO_2 ratio from polar ice core samples. *Atmos. Meas. Tech.* **7,** 3825–3837 (2014).
37. Kaiser, J. *Stable Isotope Investigations of Atmospheric Nitrous Oxide* 17–21. PhD thesis, Johannes Gutenberg Univ. Mainz (2002).
38. Lisiecki, L. E. & Lisiecki, P. A. Application of dynamic programming to the correlation of paleoclimate records. *Paleoceanography* **17,** 1049 (2002).
39. Buizert, C., Sowers, T. & Blunier, T. Assessment of diffusive isotopic fractionation in polar firn, and application to ice core trace gas records. *Earth Planet. Sci. Lett.* **361,** 110–119 (2013).
40. Tans, P. P. A note on isotopic ratios and the global atmospheric methane budget. *Glob. Biogeochem. Cycles* **11,** 77–81 (1997).
41. Sowers, T., Rodebaugh, A., Yoshida, N. & Toyoda, S. Extending records of the isotopic composition of atmospheric N_2O back to 1800 AD from air trapped in snow at the South Pole and the Greenland Ice Sheet Project II ice core. *Glob. Biogeochem. Cycles* **16,** 1129 (2002).
42. Roth, R. *Modeling Forcings and Responses in the Global Carbon Cycle-Climate System: Past, Present and Future.* PhD thesis, Univ. Bern (2013).
43. Spahni, R. *et al.* Transient simulations of the carbon and nitrogen dynamics in northern peatlands: from the Last Glacial Maximum to the 21st century. *Clim. Past* **9,** 1287–1308 (2013).
44. Sitch, S. *et al.* Evaluation of ecosystem dynamics, plant geography and terrestrial carbon cycling in the LPJ dynamic global vegetation model. *Glob. Change Biol.* **9,** 161–185 (2003).
45. Joos, F. *et al.* Transient simulations of Holocene atmospheric carbon dioxide and terrestrial carbon since the Last Glacial Maximum. *Glob. Biogeochem. Cycles* **18,** GB2002 (2004).
46. Gerten, D. *et al.* Terrestrial vegetation and water balance - hydrological evaluation of a dynamic global vegetation model. *J. Hydrol. (Amst.)* **286,** 249–270 (2004).
47. Wania, R., Ross, I. & Prentice, I. C. Integrating peatlands and permafrost into a dynamic global vegetation model: 1. Evaluation and sensitivity of physical land surface processes. *Glob. Biogeochem. Cycles* **23,** GB3014 (2009).
48. Wania, R., Ross, I. & Prentice, I. C. Integrating peatlands and permafrost into a dynamic global vegetation model: 2. Evaluation and sensitivity of vegetation and carbon cycle processes. *Glob. Biogeochem. Cycles* **23,** GB3015 (2009).
49. Xu-Ri & Prentice, I. C. Terrestrial nitrogen cycle simulation with a dynamic global vegetation model. *Glob. Change Biol.* **14,** 1745–1764 (2008).
50. Xu-Ri, Prentice I. C., Spahni, R. & Niu, H. S. Modelling terrestrial nitrous oxide emissions and implications for climate feedback. *New Phytol.* **196,** 472–488 (2012).
51. Wania, R., Ross, I. & Prentice, I. C. Implementation and evaluation of a new methane model within a dynamic global vegetation model: LPJ-WHyMe v1.3.1. *Geosci. Model Dev.* **3,** 565–584 (2010).
52. Spahni, R. *et al.* Constraining global methane emissions and uptake by ecosystems. *Biogeosciences* **8,** 1643–1665 (2011).
53. Zürcher, S. *et al.* Impact of an abrupt cooling event on interglacial methane emissions in northern peatlands. *Biogeosciences* **10,** 1963–1981 (2013).
54. Pfeiffer, M., van Leeuwen, J., van der Knaap, W. O. & Kaplan, J. O. The effect of abrupt climatic warming on biogeochemical cycling and N_2O emissions in a terrestrial ecosystem. *Palaeogeogr. Palaeoclimatol. Palaeoecol.* **391,** 74–83 (2013).
55. He, F. *Simulating Transient Climate Evolution of the Last Deglaciation with CCSM3.* PhD thesis, Univ. Wisconsin-Madison (2011).
56. Mitchell, T. D. & Jones, P. D. An improved method of constructing a database of monthly climate observations and associated high-resolution grids. *Int. J. Climatol.* **25,** 693–712 (2005).
57. Joos, F. & Spahni, R. Rates of change in natural and anthropogenic radiative forcing over the past 20,000 years. *Proc. Natl Acad. Sci. USA* **105,** 1425–1430 (2008).
58. Berger, A. L. Long-term variations of daily insolation and quaternary climatic changes. *J. Atmos. Sci.* **35,** 2362–2367 (1978).
59. Peltier, W. R. Global glacial isostasy and the surface of the ice-age Earth: The ICE-5G (VM2) model and GRACE. *Annu. Rev. Earth Planet. Sci.* **32,** 111–149 (2004).
60. Kim, K.-R. & Craig, H. Two-isotope characterization of N_2O in the Pacific Ocean and constraints on its origin in deep water. *Nature* **347,** 58–61 (1990).
61. Yoshinari, T. *et al.* Nitrogen and oxygen isotopic composition of N_2O from suboxic waters of the eastern tropical North Pacific and the Arabian Sea—measurement by continuous-flow isotope-ratio monitoring. *Mar. Chem.* **56,** 253–264 (1997).
62. Kim, K.-R. & Craig, H. Nitrogen-15 and oxygen-18 characteristics of nitrous oxide: a global perspective. *Science* **262,** 1855–1857 (1993).
63. Pérez, T. *et al.* Isotopic variability of N_2O emissions from tropical forest soils. *Glob. Biogeochem. Cycles* **14,** 525–535 (2000).
64. Rahn, T. & Wahlen, M. Stable isotope enrichment in stratospheric nitrous oxide. *Science* **278,** 1776–1778 (1997).
65. Röckmann, T. *et al.* Isotopic enrichment of nitrous oxide ($^{15}N^{14}NO$, $^{14}N^{15}NO$, $^{14}N^{14}N^{18}O$) in the stratosphere and in the laboratory. *J. Geophys. Res.* **106,** 10403–10410 (2001).

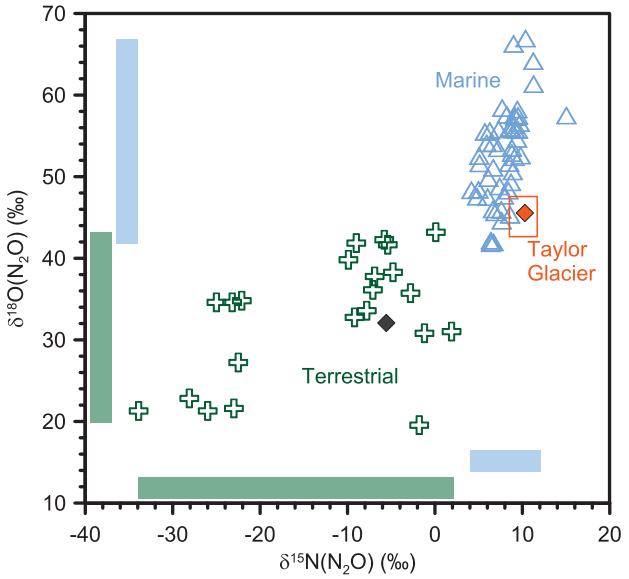

Extended Data Figure 1 | Isotopic composition of marine and terrestrial N_2O sources. Field data of $\delta^{15}N$ (relative to atmospheric N_2) and $\delta^{18}O$ (relative to VSMOW) of marine (blue triangles[60,61]) and terrestrial (green crosses[62,63]) N_2O sources. Blue and green bars indicate the ranges as used in the box model (Extended Data Table 2). The mean tropospheric value of all Taylor Glacier data (orange diamond, with the orange box indicating the full range of the data) is enriched in heavy isotopes in both $\delta^{15}N$ and $\delta^{18}O$ relative to the approximate corresponding isotopic composition of the total source (black diamond) owing to the fractionation by the stratospheric sink.

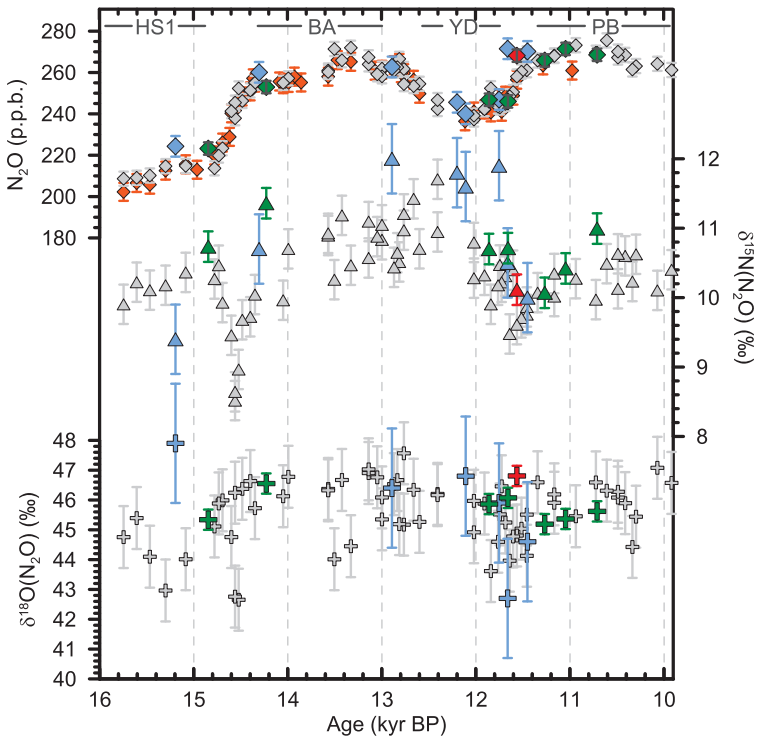

Extended Data Figure 2 | Comparison of Taylor Glacier and other data. N_2O concentration (diamonds), $\delta^{15}N$ (triangles) and $\delta^{18}O$ (crosses) data from Taylor Glacier (from the apparatus for N_2O isotopes in grey, and from the apparatus for CO_2 isotopes[36] in orange) compared with a Taylor Glacier intercomparison measurement (red) and Talos Dome data (green) from the University of Bern, and with published data from Taylor Dome (blue[4]). Taylor Glacier and Talos Dome data from the University of Bern were corrected by +2.28 p.p.b. for the N_2O concentration, −0.80‰ for $\delta^{15}N$ and +0.36‰ for $\delta^{18}O$ on the basis of intercalibration measurements made by Oregon State University and the University of Bern using firn air (Methods). The Taylor Glacier $\delta^{18}O$ data from Oregon State University (grey crosses) were corrected by +1.38‰ on the basis of measurements with bubble-free ice and NOAA-1 standard gas (Extended Data Fig. 7c and Methods). Error bars indicate $\pm 1\sigma$.

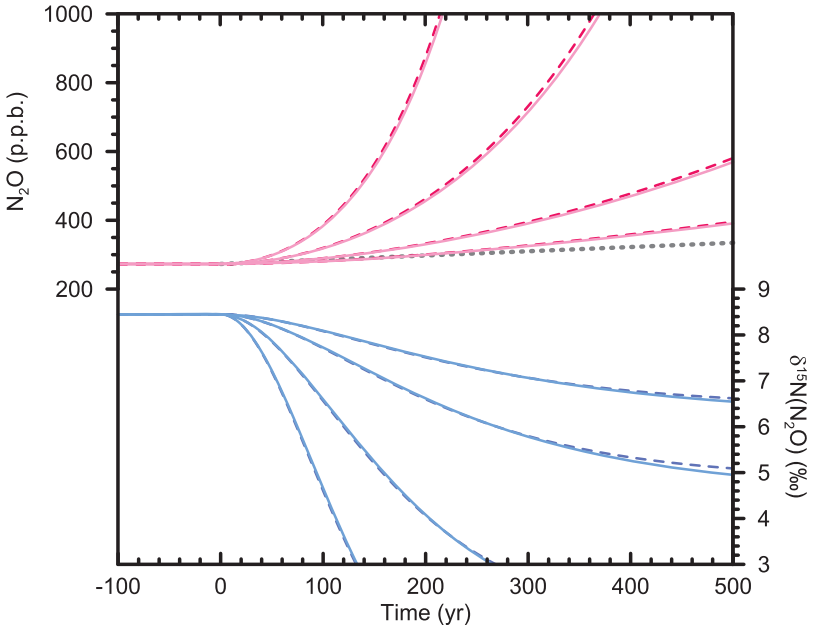

Extended Data Figure 3 | Effect of marine N_2O cycle and inventory on tropospheric N_2O concentration and $\delta^{15}N$ under changing emissions. Response of tropospheric N_2O and $\delta^{15}N$ to exponential increases in N_2O emissions with timescales of 100, 200, 500 and 1,000 yr (from left to right; the maximum increase rate in the Taylor Glacier N_2O data is indicated by the dotted grey line). Results from the two-box model (dashed lines show results without explicit representation of the ocean) are very similar to the results from the extended box model (with ocean, solid lines; Methods). The marine and terrestrial emissions are increased in parallel, that is, the marine fraction is always 37% of the total N_2O emissions and the isotopic composition of emitted N_2O remains constant. The decrease in $\delta^{15}N$ is caused by imbalances between the sources and the stratospheric sink.

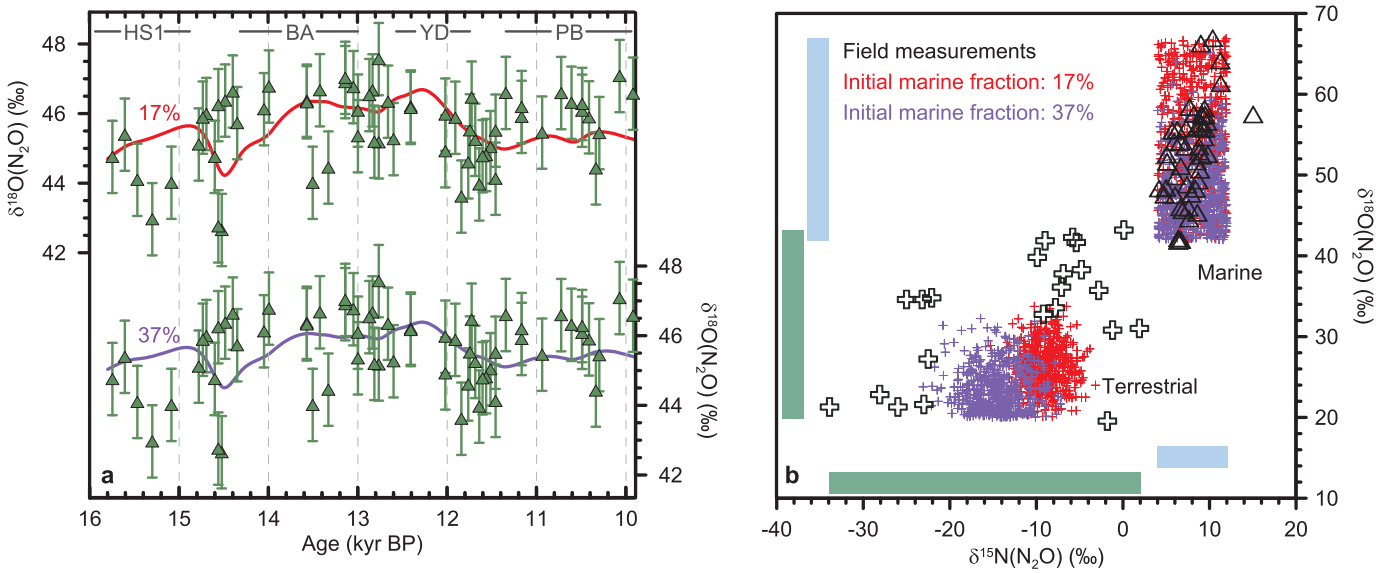

Extended Data Figure 4 | Consistency of the calculated marine and terrestrial emissions with the Taylor Glacier $\delta^{18}O$ data. **a**, $\delta^{18}O$ evolution for different initial marine fractions (red, 17%; purple, 37%) of the total emissions when calculated using the marine and terrestrial N_2O emissions determined on the basis of the Taylor Glacier N_2O concentration and $\delta^{15}N$ data. In a Monte Carlo approach only scenarios with the same mean value as the Taylor Glacier $\delta^{18}O$ data (green, with $\pm 1\sigma$ error bars) were considered, which narrowed the possible $\delta^{18}O$ isotopic composition of the sources. **b**, $\delta^{15}N$ and $\delta^{18}O$ of marine (triangles) and terrestrial (crosses) sources from modern field data (black, as in Extended Data Fig. 1), as well as the values needed to explain the Taylor Glacier data with different initial (at 16 kyr BP) marine fractions (red, 17%; purple, 37%). An initial marine fraction of 74% would require $\delta^{18}O$ isotopic compositions outside the observed range (Extended Data Table 2), suggesting that such a high marine fraction is rather unlikely. Note that the Taylor Glacier data can be explained for an initial marine fraction of 74% when considering $\delta^{15}N$ only, but only with rather extreme model parameters (Extended Data Fig. 5).

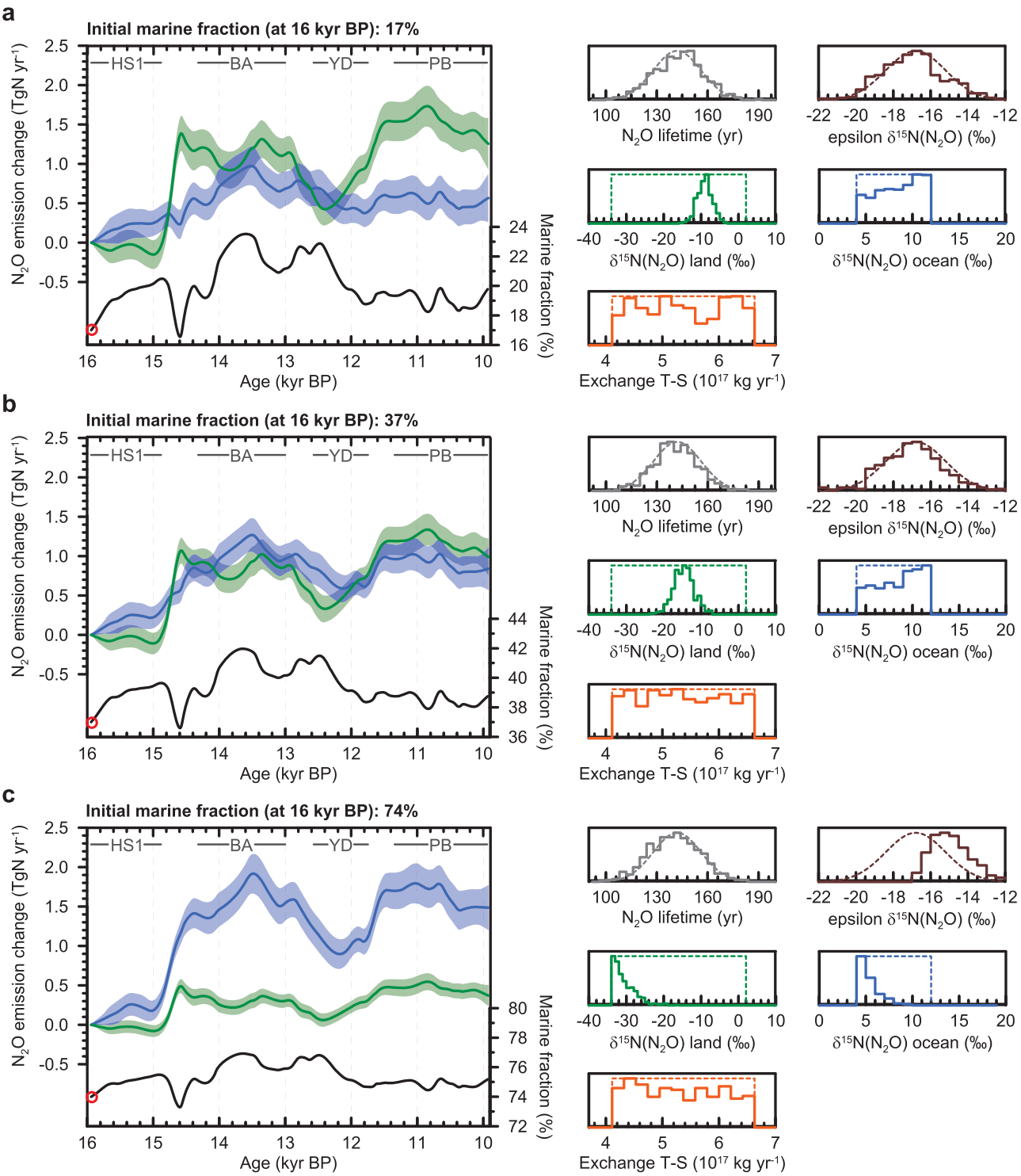

Extended Data Figure 5 | Evolution of marine and terrestrial N_2O emissions under different scenarios. Sensitivity of marine (blue in large panels) and terrestrial (green in large panels) N_2O emissions to initial marine fractions (red circles at 16 kyr BP) set to 17% (**a**), 37% (**b**) and 74% (**c**) in accordance with low, best and high estimates of the modern natural N_2O budget[1]. The uncertainty bands related to the emissions (blue and green shaded areas) result from the Monte Carlo approach and indicate $\pm 1\sigma$ of all solutions. For all scenarios, the maximum absolute changes in the marine fractions (black in large panels) over the last deglaciation are 7% or less. Dashed lines in the small panels show the distributions of the parameters as allowed for in the Monte Carlo approach (priors; Extended Data Table 2), and solid lines indicate the distributions of the parameters which allow for a reproduction of the Taylor Glacier N_2O concentration and $\delta^{15}N$ that respects the prescribed initial marine fractions (posteriors).

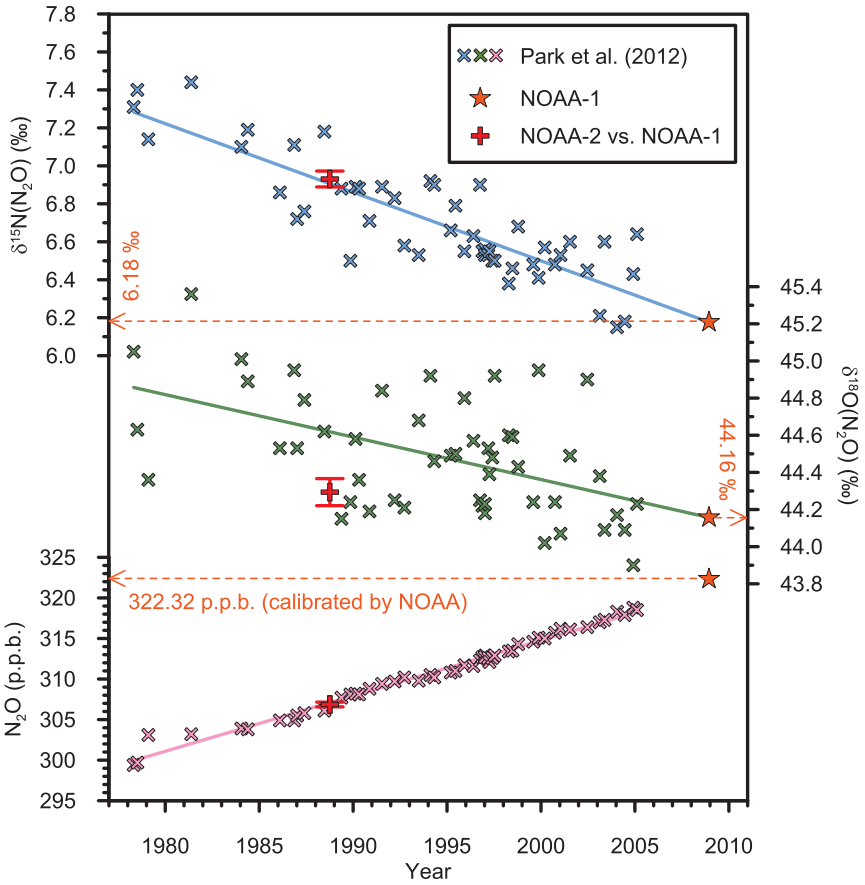

Extended Data Figure 6 | Standard gases for $\delta^{15}N$, $\delta^{18}O$ and N_2O concentration. The $\delta^{15}N$ and $\delta^{18}O$ values of 6.18‰ and 44.16‰ of the NOAA-1 standard gas collected at Niwot Ridge, Colorado, were assigned by linear extrapolation of the data from Cape Grim, Tasmania[31], to the collection date of NOAA-1 (11 December 2008), on the basis of the assumption that N_2O and its isotopes are well mixed in the troposphere owing to the rather long atmospheric lifetime. The N_2O concentration of 322.32 ± 0.14 p.p.b. of the NOAA-1 standard gas was directly determined by the National Oceanic and Atmospheric Administration (NOAA-2006A scale; linear extrapolation of the Cape Grim data would lead to 320.9 p.p.b.). To test the calibrations for the N_2O concentration and isotopic compositions, a second standard gas, NOAA-2, which was collected at Niwot Ridge on 5 October 1988, was measured against NOAA-1. The results (red crosses) were in good agreement with the Cape Grim data, in particular when taking into account the interannual scatter observed in the archived air.

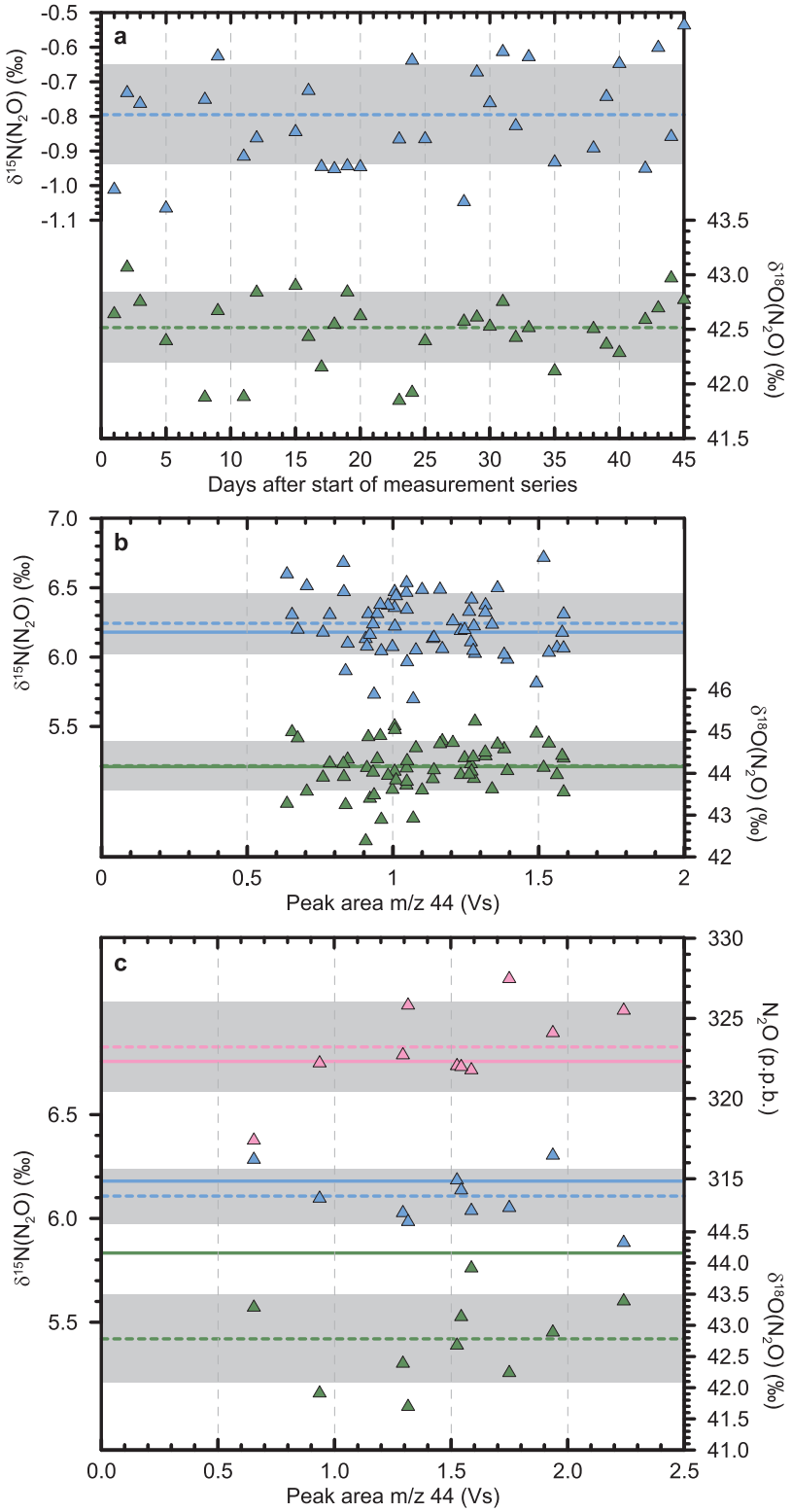

Extended Data Figure 7 | Stability in the course of the measurement series, characterization of the amount dependency of the measurement system, and tests with bubble-free ice. **a**, NOAA-3 standard gas measurements performed at the end of each measurement day. No significant drifts were observed in the course of the measurement series, and the standard deviations for $\delta^{15}N$ and $\delta^{18}O$ were respectively 0.14‰ and 0.32‰ ($n = 31$), as indicated by the grey areas ($\pm 1\sigma$) around the means (dashed lines). **b**, NOAA-1 standard gas measurements resulting in similar peak areas to the preceding ice-sample measurement routinely performed throughout the measurement series. These measurements covering the full range of peak areas from ice samples did not reveal any significant amount dependency. The mean and standard deviation (dashed lines and grey areas) for $\delta^{15}N$ were 6.24‰ ± 0.22‰ and those for $\delta^{18}O$ were 44.18‰ ± 0.59‰ ($\pm 1\sigma$, $n = 58$), in agreement with the expected values (solid lines). **c**, Measurements of different amounts of NOAA-1 standard gas which was stored in the extraction pots while pieces of bubble-free ice were grated. Dashed lines and grey areas indicate the means and standard deviations ($\pm 1\sigma$, $n = 10$), and solid lines indicate the expected values. On the basis of these measurements with bubble-free ice and the results shown in **b**, N_2O, $\delta^{15}N$ and $\delta^{18}O$ were not corrected for amount dependency. However, during the extraction of standard gas over ice, a −1.38‰ offset was introduced in $\delta^{18}O$. Accordingly, all Taylor Glacier $\delta^{18}O$ values were corrected by +1.38‰.

Extended Data Table 1 | Equations forming the basis of the two-box model used to calculate marine and terrestrial N_2O emissions

$$\frac{dM_{N_2O,trop}}{dt} = \underbrace{F_{ocean} + F_{land}}_{F_{total}} + Ex_{trop,strat}\left([N_2O]_{strat} - [N_2O]_{trop}\right) \quad (1)$$

$$\frac{dM_{N_2O,strat}}{dt} = Ex_{trop,strat}\left([N_2O]_{trop} - [N_2O]_{strat}\right) - F_{sink} \quad (2)$$

$$F_{sink} = \frac{M_{N_2O,strat}}{k_{strat}} \quad \text{with} \quad k_{strat} = \tau_{N_2O}\chi_{strat} - \frac{M_{atm}}{Ex_{trop,strat}}\chi_{strat}(1-\chi_{strat}) \quad (3)$$

$$\frac{d(M_{N_2O,trop}R_{trop})}{dt} = fF_{total}R_{ocean} + (1-f)F_{total}R_{land} + Ex_{trop,strat}([N_2O]_{strat}R_{strat} - [N_2O]_{trop}R_{trop}) \quad (4)$$

$$\frac{d(M_{N_2O,strat}R_{strat})}{dt} = Ex_{trop,strat}([N_2O]_{trop}R_{trop} - [N_2O]_{strat}R_{strat}) - F_{sink}R_{strat}\left(\frac{\varepsilon}{1000} + 1\right) \quad (5)$$

Parameters (see also Extended Data Table 2): M_{atm}, the total mass of the atmosphere; χ_{strat}, the stratospheric fraction of the total atmosphere; $M_{N_2O,trop}$ and $M_{N_2O,strat}$, the masses of N_2O in the troposphere and stratosphere; F_{ocean} and F_{land}, the marine and terrestrial N_2O emissions; $Ex_{trop,strat}$, the rate of exchange of air between troposphere and stratosphere; $[N_2O]_{trop}$ and $[N_2O]_{strat}$, the N_2O mass concentrations in the troposphere and stratosphere; F_{sink}, the rate of removal of N_2O from the stratosphere; τ_{N_2O}, the atmospheric lifetime of N_2O in equilibrium; k_{strat}, the stratospheric lifetime of N_2O; f and $1-f$, the marine and terrestrial fractions of total N_2O emissions; ε, the fractionation constant of the stratospheric sink as defined in ref. 64; R_{trop} and R_{strat}, the isotopic ratios in the troposphere and in the stratosphere; R_{ocean} and R_{land}, the isotopic ratios of marine and terrestrial emissions.

Extended Data Table 2 | Parameters for the two-box model used to calculate marine and terrestrial N_2O emissions

Parameter	Range	Unit	Distribution	Reference
Lifetime	142±14	yr	Gaussian	Ref. 12
$\delta^{15}N(N_2O)$ marine	[4; 12]	‰	Uniform	See Extended Data Figure 1
$\delta^{15}N(N_2O)$ terrestrial	[-34; 2]	‰	Uniform	See Extended Data Figure 1
$\delta^{18}O(N_2O)$ marine	[42; 67]	‰	Uniform	See Extended Data Figure 1
$\delta^{18}O(N_2O)$ terrestrial	[20; 43]	‰	Uniform	See Extended Data Figure 1
Stratospheric fractionation constant (^{15}N)	-16.8±1.6	‰	Gaussian	Ref. 65
Stratospheric fractionation constant (^{18}O)	-13.8±2.0	‰	Gaussian	Ref. 65
Number of moles in atmosphere	$1.77x10^{20}$	mol	Constant	As in ref. 10
Stratospheric fraction of total atmosphere	0.15	-	Constant	As in ref. 10
Exchange rate troposphere/stratosphere	[$4.11x10^{17}$; $6.63x10^{17}$]	kg yr^{-1}	Uniform	As in ref. 9